Inorganic Chemistry

Article

pubs.acs.org/IC

# Inducing Single Molecule Magnetic Behavior in a $[Co_4O_4]$ Cubane via a Pronounced Solvatomagnetic Effect

Felix J. Klinke, Animesh Das, Serhiy Demeshko, Sebastian Dechert, and Franc Meyer*

Institute of Inorganic Chemistry, Georg-August-University, Tammannstrasse 4, D-37077 Göttingen, Germany

Supporting Information

**ABSTRACT:** The pyrazole-based tridentate diol ligand 2-(1-(2-hydroxyethyl)-1*H*-pyrazol-3-yl)phenol ($H_2L$) forms a cubane-type complex $[Co_4L_4(MeOH)_4]$ (**1**) that features a $\{Co_4O_4\}$ core and four exogenous MeOH ligands. Electrospray ionization mass spectrometry suggests that the MeOH ligands are easily lost, and thermogravimetric analysis evinces a thermally induced release of those methanol molecules from solid material in the temperature range from 380 to 440 K. Desolvation was found to give rise to a pronounced solvatomagnetic effect that causes a switching of the spin ground state of the $\{Co_4O_4\}$ core from diamagnetic to magnetic. Furthermore, the desolvated "naked" $[Co_4L_4]$ cube (**1***) shows slow relaxation of the magnetization and butterfly-like magnetic hysteresis at 2 K. A comparatively high relaxation barrier $U_{eff}/k_B$ = 64.4 K and a characteristic relaxation time $\tau_0 = 3.8 \times 10^{-9}$ s for **1*** have been derived from an Arrhenius plot. These findings thus demonstrate that the emergence of interesting magnetic properties in molecule-based materials can be triggered via a solvatomagnetic process, even for materials that in their solvated form have a diamagnetic ($S_T$ = 0) ground state.

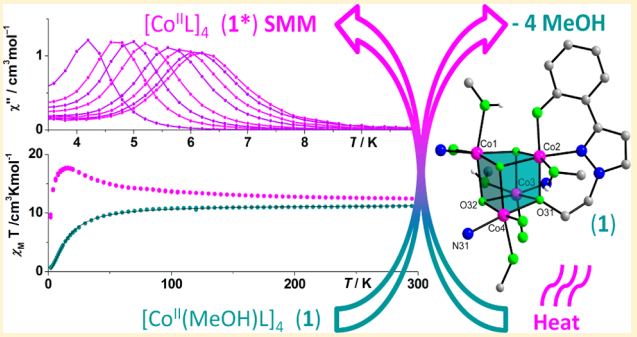


## INTRODUCTION

Molecular magnetism has been a vibrant research field for the last two decades, since molecule-based materials allow for combining useful magnetic responses with other properties characteristic for molecular compounds to generate phenomena that cannot be achieved with conventional magnets.[1] One such phenomenon, which is of great interest for sensing applications, is the so-called solvatomagnetic effect (SME), that is, the switching of magnetic properties by the uptake, exchange, or release of solvent molecules in molecule-based materials.[2,3] Most compounds showing an SME are either coordination polymers or metal organic frameworks, and often changes in their structural dimensionality upon solvent influence are involved.[4] Only a few examples are known of compounds showing SME while remaining truly molecular systems.[5−9] Two of these examples exhibit changes in already-existent single molecule magnet (SMM) behavior upon release of crystal or weakly bonded water molecules.[5,9] In a previous report we introduced the tetranuclear cubane-type complex $[Ni_4L_4(MeOH)_4]\cdot H_2O$ that shows a dramatic SME, namely a switching of the spin ground state from $S$ = 4 to $S$ = 0 induced by the exchange of coordinated solvent molecules (MeOH versus $H_2O$).[8] In the present work we now expand this concept to show that (i) our ligand system 2-(1-(2-hydroxyethyl)-1*H*-pyrazol-3-yl)phenol ($H_2L$) (Scheme 1) is able to form cubane-type complexes with further transition metal ions like cobalt(II) and (ii) even more importantly that the resulting complex $[Co_4L_4(MeOH)_4]$ (**1**) exhibits switching of the spin ground state from diamagnetic to magnetic and furthermore becomes an SMM upon release of the coordinated methanol molecules. While some cubane-type cobalt complexes with SMM properties have been published,[9−11] this appears to be the first report of a molecular system where SMM behavior is triggered via the solvatomagnetic effect.

## RESULTS AND DISCUSSION

**Synthesis and Structural Characterization of the Complexes.** The ligand $H_2L$ was reacted with 1 equiv of $Co(ClO_4)_2\cdot 6H_2O$ and 2 equiv of $NEt_3$ as base in dry methanol under inert conditions to give complex **1** as a brown precipitate via a self-assembly process (Scheme 1); complex **1** was then recrystallized by layering a $CH_2Cl_2$ solution of **1** with *n*-hexane. Light-brown single crystals suitable for X-ray structure analysis were obtained in the same way after several days. The molecular structure of **1**, determined by X-ray crystallography, is shown in Figure 1. Selected interatomic distances and angles are compiled in the Supporting Material and in Table 1.

Four cobalt atoms and four oxygen atoms constitute the distorted cubane-type $\{Co_4O_4\}$ core, the coordination sphere of each metal atom being completed by the phenolate O and pyrazole N from the dianionic ligand, as well as by an exogenous methanol ligand. Thus all cobalt(II) ions are six-coordinate in a distorted octahedral coordination environment. Similar to what was observed in the previously published $[Ni_4L_4(solv)_4]$ compounds, the four exogenous MeOH ligands serve as hydrogen bond donors toward the phenolate O.

**Received:** November 5, 2013
**Published:** February 27, 2014

 © 2014 American Chemical Society  dx.doi.org/10.1021/ic4027656 | *Inorg. Chem.* 2014, 53, 2976−2982

**Scheme 1. Synthesis and Topology of 1 and 1*[a]**

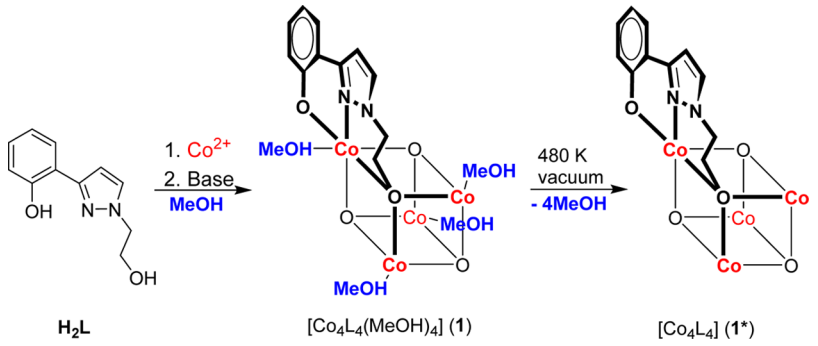


[a]For clarity only one ligand $L^{2-}$ and its coordination mode (bold) at the $\{Co_4(\mu_3\text{-}O)_4\}$ core are shown.

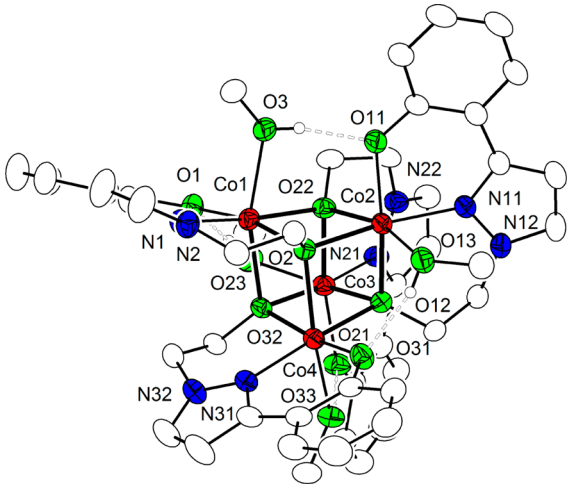


**Figure 1.** Molecular structure of complex **1** (thermal ellipsoids drawn at the 30% probability level). Most hydrogen atoms have been omitted. Only one of the two crystallographically independent molecules is shown.

**Table 1. Co−O−Co Angles (deg) for Complex 1[a]**

| M−O−M | 1 |
|---|---|
| $Co_A$−$O_{A2}$−$Co_B$ | 99.07(13)/98.24(12) |
| $Co_A$−$O_{C2}$−$Co_B$ | 93.90(11)/93.19(12) |
| $Co_A$−$O_{C2}$−$Co_C$ | 97.98(13)/98.11(13) |
| $Co_A$−$O_{D2}$−$Co_C$ | 93.61(11)/93.35(12) |
| $Co_A$−$O_{A2}$−$Co_D$ | 101.06(11)/101.63(14) |
| $Co_A$−$O_{D2}$−$Co_D$ | 101.21(11)/100.82(14) |
| $Co_B$−$O_{B2}$−$Co_C$ | 100.83(13)/100.01(11) |
| $Co_B$−$O_{C2}$−$Co_C$ | 101.94(13)/100.71(12) |
| $Co_B$−$O_{A2}$−$Co_D$ | 93.75(11)/94.15(12) |
| $Co_B$−$O_{B2}$−$Co_D$ | 97.43(13)/99.07(13) |
| $Co_C$−$O_{B2}$−$Co_D$ | 92.49(11)/94.50(12) |
| $Co_C$−$O_{D2}$−$Co_D$ | 98.71(12)/98.14(13) |
| av M−O−M (**SF**) | 95.87/96.09 |
| av M−O−M (**OF**) | 101.26/100.79 |

[a]See Figure 2 for numbering scheme.

Thus four faces of the $\{Co_4O_4\}$ cube (denoted as side faces, **SF**) are spanned by O−H···O hydrogen bonds, while the two remaining faces, which are located at opposite sides of the cube (denoted **OF** and colored in blue in Figure 2), are not bridged. This leads to distinct bond lengths and angles for the two different types of cube faces **SF** and **OF** (Table 1 and Supporting Information, Table S3). In particular, bond angles at the bridging oxygen atoms are significantly more acute along the faces spanned by O−H···O hydrogen bonds (**SF**), resulting in shorter Co···Co distances and deformation of the cubane core away from ideal cubic symmetry. A detailed discussion of these structural differences and their relevance for magneto structural correlations was presented earlier for closely related nickel cubanes[8] and is not part of the present work. However, structural perturbation is a crucial factor determining the magnetic exchange interactions through O-atom bridges in cobalt cubanes as well,[12] and this issue will be addressed below when coupling pathways are discussed.

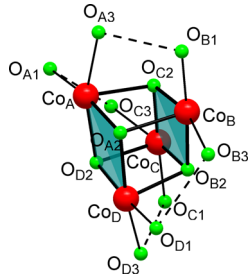


**Figure 2.** Emphasis of the cubane-like $\{Co_4O_4\}$ fragment and hydrogen bonding interactions in **1**. Blue faces (**OF**) are not spanned by hydrogen bonds. Complex **1** (two crystallographically independent molecules): $Co_A$= Co1/Co11, $O_{A1}$ = O1/O41, $O_{A2}$ = O2/O42, $O_{A3}$ = O3/O43, $Co_B$ = Co2/Co12, $O_{B1}$ = O11/O51, $O_{B2}$ = O12/O52, $O_{B3}$ = O13/O53, $Co_C$ = Co3/Co13, $O_{C1}$ = O21/O61, $O_{C2}$ = O22/O62, $O_{C3}$ = O23/O63, $Co_D$ = Co4/Co14, $O_{D1}$ = O31/O71, $O_{D1}$ = O32/O72, $O_{D3}$ = O33/O73.

**Thermogravimetric Analysis.** In view of the potentially labile MeOH solvent molecules in complex **1**, and since we were interested in potential solvatomagnetic effects of the $\{Co_4O_4\}$ cubane complex, we investigated the thermal degradation of solid **1** and accompanying changes in its composition by thermogravimetric (TGA) and elemental analysis (EA). TGA revealed that **1** smoothly loses all coordinated methanol molecules in one step in the temperature range of 380−440 K. Then a stable plateau occurs that lasts to 700 K (Figure 3). The mass loss of about 10.8% until 440 K corresponds well with the calculated value for loss of four MeOH molecules (10.9%). The release of all solvent molecules from the cobalt cube was also confirmed by EA of powdered material directly after the thermogravimetric measurements; Anal. Calcd (%) for $C_{44}H_{40}Co_4N_8O_8$: C 50.59, H 3.86, N 10.73. Found: C 50.47, H, 3.91, N 10.65. Interestingly, the


dx.doi.org/10.1021/ic4027656 | Inorg. Chem. 2014, 53, 2976−2982

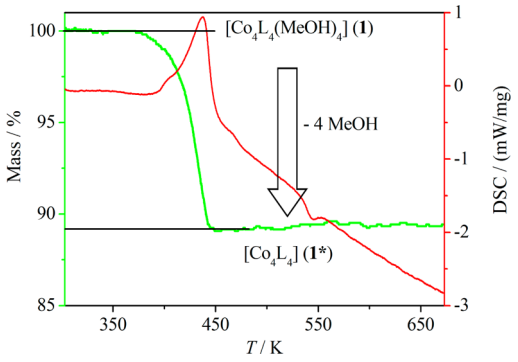


**Figure 3.** Thermogravimetric analysis of **1**, scan rate 10 K/min.

temperature range for the loss of all coordinated methanol molecules in **1** is comparable to the release of guest water molecules in some recently reported $Ni_7$ and $Co_7$ cluster-based polymers; however, in the case of molecule-based **1** the process is more abrupt.[13] Differential scanning calorimetry (DSC) measurements performed simultaneously with the TGA revealed a relatively broad endothermic event beginning right after at the onset of the mass loss at about 380 K with a maximum at 438 K and $\Delta H$ = 276 kJ $mol^{-1}$.

The information obtained from TGA was then used for the preparative synthesis of the "naked" cubane **1*** that does not contain any coordinated solvent molecules by grinding crystalline material of complex **1** and heating those samples under vacuum conditions slowly to 480 K (Scheme 1). The release of all solvent molecules was confirmed by EA, and the desolvation process was accompanied by a slight color change from brown (**1**) to beige (**1***). Unfortunately, no structural information for **1*** is available, since desolvation of **1** inevitably goes along with loss of crystallinity of the material; all attempts to achieve a single-crystal-to-single-crystal (SCSC) transformation failed. Furthermore it seems unlikely that crystallization of the desolvated complex that lacks any additional solvent ligands can be achieved via solution methods. However, desolvated **1*** is reproducible prepared via the described method, namely, by thermal treatment of solid **1**, which allowed for studying its magnetic properties by superconducting quantum interference device (SQUID) magnetometry (see below).

**ESI Mass Spectrometry.** This method was used to gain further information about the composition and stability of **1** and **1***. If kept in a strictly air- and moisture-free environment, solid **1*** proved to be stable: ESI-MS experiments of MeCN solutions of **1*** showed the intact $\{Co_4O_4\}$ cubane core even after storage for several weeks in the glovebox (Figure 4).

Both the original compound **1** and the desolvated complex **1***, when dissolved in dry MeCN, gave nearly identical ESI-MS spectra in positive-ion mode. The main peak in the spectra corresponds to the singly charged $[Co_4L_4H]^+$ fragment of the protonated complex without any solvent molecules ($m/z$ = 1045.2 (**1** + H), 1045.1 (**1*** + H)), which is overlaid with the singly oxidized form $[Co_4L_4]^+$ generated in the mass spectrometer. Simulations of the isotopic distribution for both fragments are included in Figure 4 and show good agreement with the experimental spectrum. These experiments prove not only the stability and existence of the $\{Co_4L_4\}$ core in solution, but also reveal the in situ formation of **1*** from **1** under ESI-MS conditions, namely, the lability of the exogenous MeOH ligands.

**Static Magnetic Properties.** Magnetic susceptibility data were collected for complexes $[Co_4L_4(MeOH)_4]$ (**1**) and

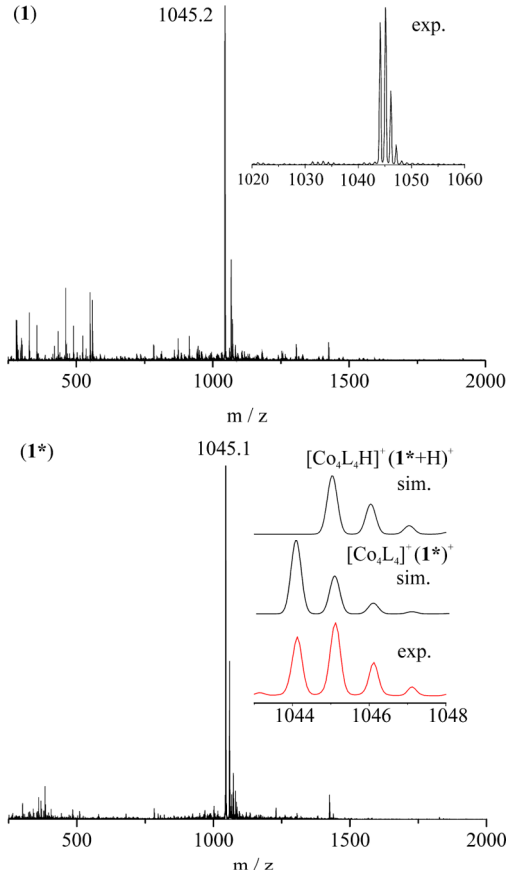


**Figure 4.** Positive-ion ESI-MS spectrum of (top) **1** and (bottom) **1*** in MeCN; the upper inset shows a magnification of the experimental spectrum for **1**, and the lower inset shows a magnification of the experimental spectrum for **1*** and simulations of the major peak at 1045 $m/z$. The protonated complex peak $[Co_4L_4H]^+$ is overlaid with the singly oxidized form $[Co_4L_4]^+$ generated in the mass spectrometer.

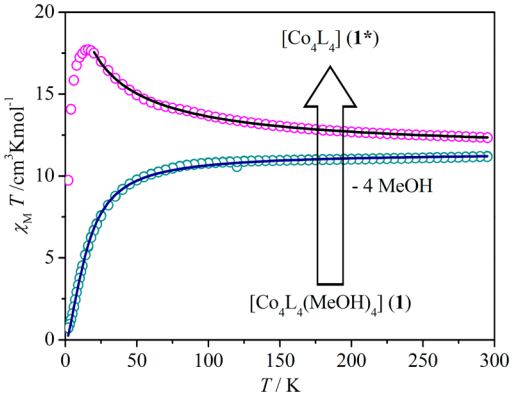


**Figure 5.** Temperature dependence of $\chi_M T$ for **1** and **1***; solid lines represent the best simulations according to eq 1, with fit parameters given in Table 2.

$[Co_4L_4]$ (**1***) in the temperature range from 295 to 2.0 K. Figure 5 shows the plot of $\chi_M T$ versus temperature and illustrates the striking differences in the magnetic properties for cubane-type complexes with and without coordinated solvent molecules.

For **1** the product $\chi_M T$ decreases only slightly from 295 to 100 K and then drops more steeply to reach a minimum value close to zero at very low temperatures, indicating an $S_T$ = 0


dx.doi.org/10.1021/ic4027656 | Inorg. Chem. 2014, 53, 2976−2982

ground state (Figure 5, blue circles). In contrast, the $\chi_M T$ curve of **1*** increases upon lowering the temperature to reach a maximum of 17.7 $cm^3$ K $mol^{-1}$ at 16 K (Figure 5, magenta circles), evidencing a high-spin ground state for the naked cube.

According to the structural information available for **1**, experimental magnetic data for both complexes were initially simulated using a fitting procedure to the appropriate Heisenberg–Dirac–van Vleck (HDvV) spin Hamiltonian for two isotropic exchange coupling constants (Figure 6, left) and

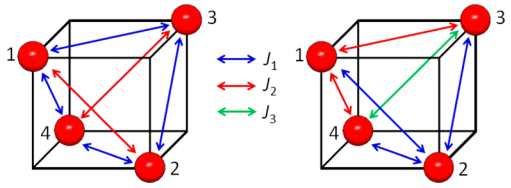


**Figure 6.** Magnetic coupling schemes for (left) two and (right) three independent coupling constants. In the first case, constant $J_2$ marked in red describes the pathway across faces not spanned by hydrogen bonds (**OF**, Figure 2).

Zeeman splitting (eq 1).[14] Thereby, $J_1$ represents the interaction via bridged faces (**SF**), and $J_2$ represents the interaction via open faces (**OF**) (see Synthesis and Structural Characterization of the Complexes for definitions of **SF** and **OF**).

$$\hat{H} = -2J_1(\hat{S}_1\hat{S}_3 + \hat{S}_1\hat{S}_4 + \hat{S}_2\hat{S}_3 + \hat{S}_2\hat{S}_4) - 2J_2(\hat{S}_1\hat{S}_2 + \hat{S}_3\hat{S}_4) + g\mu_B\vec{B}\sum_{i=1}^{4}\vec{S}_{zi} \quad (1)$$

Figure 5 shows the simulations with best-fit parameters obtained using this model (solid lines); values are given in Table 2. While the antiferromagnetic coupling constant $J_2$ is almost the same for both complexes, the ferromagnetic constant $J_1$ is an order of magnitude higher for **1*** than it is for **1**, which translates into the change of the spin ground state from diamagnetic to magnetic. If classified according to the shape of the $\chi_M T$ curve, all cobalt(II) cubane complexes can be grouped into three classes, one of which has the typical signatures found for **1** with dominant antiferromagnetic interaction (class B).[12] Surprisingly, complexes of this class are rather rare in literature, and we could find only two examples[15,16] that exhibit the same shape of the $\chi_M T$ curve; however, no magnetic analysis was presented or magnetic data were only given for temperatures higher than 100 K. It thus appears that **1** is the first example of a cobalt(II) type B cubane that has been magnetically analyzed over a wide temperature range.

For **1*** magnetic data simulation was only accurate in the temperature range from room temperature to 20 K when using the model with two $J$ parameters (eq 1). Even after including zero-field splitting, the experimental data for **1*** could not be reproduced well over the full temperature range when using two $J$ coupling constants only. We thus assume that upon release of all MeOH ligands the $\{Co_4O_4\}$ core undergoes structural distortion and reduction in symmetry, meaning that more complicated coupling schemes are needed to properly describe the system. Since no detailed solid-state structural information is available for **1***, an arbitrarily selected model with three $J$ parameters, based on a reduced $C_s$ symmetric coupling scheme, and with zero field splitting (Figure 6 right, eq 2) was applied to achieve a reasonable (though far from perfect) description over the whole temperature range. The result of this fit is displayed in Figure 7 and confirms the higher

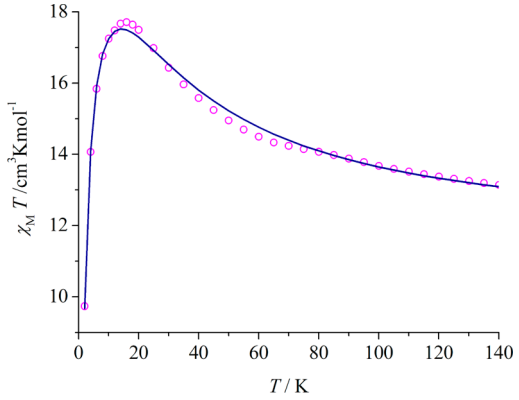


**Figure 7.** Magnetic susceptibility data for **1*** at 0.5 T; the solid line represents a simulation using best-fit parameters with $J_1$, $J_2$, and $J_3$ according to eq 2; see text and Table 2 for details.

degree of distortion in **1***, regardless of the exact type of distortion.

$$\hat{H} = -2J_1(\hat{S}_1\hat{S}_2 + \hat{S}_2\hat{S}_3 + \hat{S}_2\hat{S}_4) - 2J_2(\hat{S}_1\hat{S}_3 + \hat{S}_1\hat{S}_4) - 2J_3\hat{S}_3\hat{S}_4 + g\mu_B\vec{B}\sum_{i=1}^{4}\vec{S}_i + D\sum_{i=4}^{4}(\hat{S}_{zi}^{\,2} - S_i(S_i+1)/3) \quad (2)$$

The fitting parameters illustrate that ferromagnetic as well as antiferromagnetic couplings are operative in both $\{Co_4O_4\}$ complexes; however, in **1*** the ferromagnetic interaction dominates. Switching of the ground state after release of all exogenous MeOH ligands can arise (i) from slight perturbation of the core's solid-state structure, since the bond angles at the bridging O atoms have been discussed as a major factor determining the overall magnetic coupling in the "normal" cubes[12] or (ii) from the lowering of the coordination number from six to five.[17]

**Dynamic Magnetic Properties.** Since **1*** has a high-spin ground state and cobalt(II), having a higher orbital angular momentum than previously used nickel(II), is a suitable ion to create SMMs, a more detailed study of the magnetic properties of **1*** was performed. Figure 8a shows the imaginary part (out-of-phase) of the alternating current (AC) susceptibility measurement of **1*** plotted against temperature, reflecting the

**Table 2. Best-Fit Parameters of Magnetic Data Analysis**

| complex | $g$ | $J_1$ ($cm^{-1}$) | $J_2$ ($cm^{-1}$) | $J_3$ ($cm^{-1}$) | $\|D\|$ ($cm^{-1}$) | TIP ($10^{-6}$ $cm^3$ $mol^{-1}$) |
|---|---|---|---|---|---|---|
| **1** | 2.52 | +0.56 | −2.84 | | 0 | 100 |
| **1*** | 2.48 | +5.1 | −3.87 | | 0 | 400 |
| **1***[a] | 2.48 | +5.70 | −2.69 | −1.33 | 11.76 | 400 |

[a]Alternative fit parameters obtained with additional coupling constant $J_3$ and axial zero-field splitting; see Figure 7.


dx.doi.org/10.1021/ic4027656 | Inorg. Chem. 2014, 53, 2976–2982

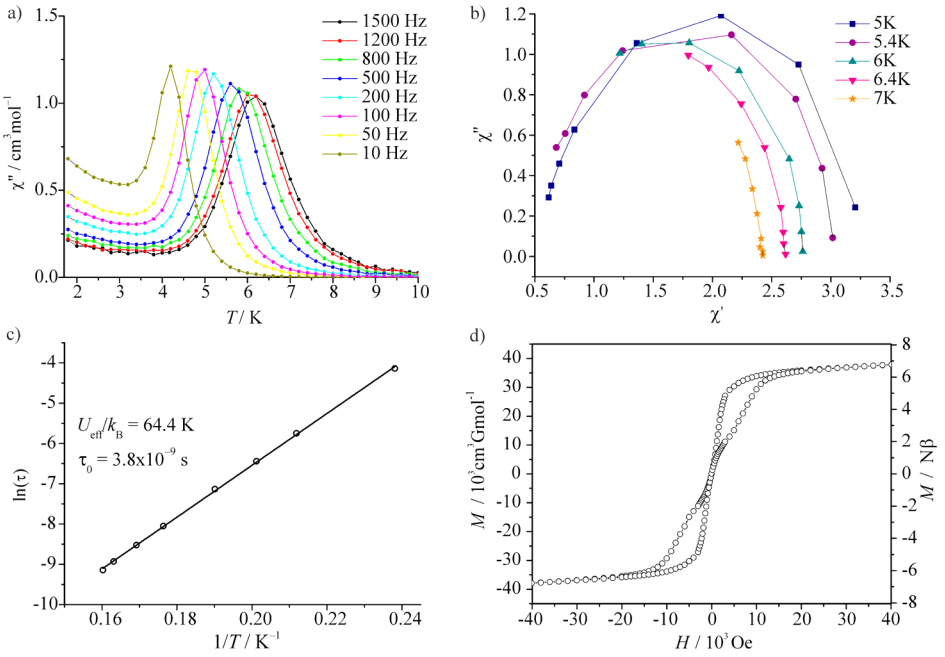


**Figure 8.** (a) AC susceptibility ($H_{AC}$ = 3 Oe) measurement of **1***, out-of-phase signal without applied DC field. (b) Cole–Cole plot generated from AC susceptibility measurement of **1*** without applied DC field. (c) Arrhenius plot generated from AC susceptibility measurement of **1*** without applied DC field. (d) Magnetic hysteresis of **1*** measured at 2 K (right).

frequency-dependent shift of the maximum of $\chi''$ for oscillating frequencies between 1500 and 10 Hz. The corresponding real (in-phase) part of the AC susceptibility $\chi'$ is provided in the Supporting Information (Figure S2).

To exclude the possibility that the frequency-dependent AC susceptibility originates from spin-glass behavior, the shift of the peak temperature ($T_p$) of the in-phase part $\chi'$ was analyzed as $\Phi = (\Delta T_p/T)/\Delta(\log \nu)$,[18] where $\nu$ is the applied frequency (in our case between 1500 and 10 Hz). The obtained value for $\Phi$ of 0.15 is 2 orders of magnitude larger than typical values expected for spin-glass systems (where $\Phi$ varies in the range of 0.004–0.018) and lies in the usual range for superparamagnets, SMMs, or SCMs.[19] Additionally, the resulting Cole–Cole plot in which $\chi''$ is plotted against $\chi'$ for all frequencies can be drawn at fixed temperatures (Figure 8b). The almost-perfect hemicycles for temperatures between 5 and 6 K indicate that there is only one active relaxation pathway.

To gain closer insight into the relaxation parameters, the data were analyzed using an Arrhenuis law for a thermally activated process: $\tau = \tau_0 \exp(U_{eff}/k_BT)$, with the energy barrier $U_{eff}/k_B$ and the relaxation time $\tau_0$.[20] Both values can be determined from a plot of $\ln(\tau)$ versus $(1/T)$. The parameter $\tau$ is calculated as $\tau = 1/2\pi\nu$, the used $T$ values are the peak temperatures of $\chi''$ at a given frequency. The Arrhenius-type plot for **1*** (Figure 8c) gives a relaxation barrier of $U_{eff}/k_B$ = 64.4 K and the characteristic relaxation time $\tau_0 = 3.8 \times 10^{-9}$ s. Few examples of cobalt cubane complexes with SMM properties are known to literature. Most of them feature relaxation barriers between 13 and 30 K,[9,10] while some rare examples show barrier heights of around 60 K.[11]

Since the value for **1*** is rather high, it was possible to observe a butterfly-like hysteresis loop at 2 K even by using a conventional SQUID magnetometer (Figure 8). The absence of any coercivity can probably be explained by very fast quantum tunneling of the magnetization at zero field, as it was also observed in similar cases for intact cobalt cubane complexes.[10b,11a] Another possible reason for the occurrence of such butterfly-like hysteresis loops might be the so-called phonon bottleneck effect,[21,22] meaning that the hysteresis occurs because of poor thermal contact of the sample with the heat bath; this has previously been observed for some spin clusters such as $V_{15}$,[23] $Fe_{12}$,[24] or $Fe_2$.[25] However, the maximum of the out-of-phase AC susceptibility $\chi''$ for those complexes is only observed upon application of an additional direct current (DC) magnetic field of 1 to 10 kOe.[22,26] For the present system **1*** this is not the case, and the maximum of the out-of-phase AC susceptibility is evident even in zero DC field. This likely excludes the possibility of phonon bottleneck effects being the cause of the observed behavior.

## CONCLUSIONS

In conclusion, thermal treatment of the new $[Co_4L_4(MeOH)_4]$ cubane complex **1** with $S_T = 0$ triggers switching of the spin ground state upon release of directly coordinated solvent molecules, leading to a high-spin ground state for the naked $[Co_4L_4]$ (**1***). Desolvated **1*** shows slow relaxation of the magnetization with a high relaxation barrier of 64.4 K. These findings add another important aspect to the chemistry of compounds with a $\{M_4O_4\}$ core, since solvent molecules are usually bound to such cubane-type complexes. It is now demonstrated that the SME offers the possibility to trigger the emergence of interesting magnetic properties via controlled release of solvent ligands even if the initial ground state of the cubane complex is diamagnetic.

## EXPERIMENTAL SECTION

**Materials and Methods.** Solvents were purified by established procedures.[27] All other chemicals were purchased from commercial sources and used as received. Microanalyses were performed by the Analytical Laboratory of the Institute for Inorganic Chemistry at Georg-August-University Göttingen using an Elementar Vario EL III. The $^1$H and $^{13}$C NMR spectra were recorded with a Bruker Avance 300 MHz spectrometer; chemical shifts for the $^1$H and $^{13}$C spectra are reported in ppm relative to residual solvent signals of $CDCl_3$ ($\delta$ =


dx.doi.org/10.1021/ic4027656 | Inorg. Chem. 2014, 53, 2976–2982

7.26 ppm and 77.16 ppm). The IR spectra were recorded using a Digilab Excalibur Series FTS 3000 spectrometer at room temperature. Mass spectra were measured using a Bruker HTC Ultra (ESI-MS) or with a Finnigan MAT 95 (EI-MS). Thermogravimetric measurements were performed using a Netzsch STA409PC LUXX, scan rate: 10 K/min. Magnetic data were measured with a Quantum-Design MPMS-XL-5 SQUID magnetometer equipped with a 5 T magnet in the range from 2 to 295 K. Samples were treated as described for the individual compounds and fixed in a nonmagnetic sample holder. Each raw data file for the measured magnetic moment was corrected for the diamagnetic contribution of the sample holder and the sample. A Curie-behaved paramagnetic impurity (PI) with spin $S = 1$ (fixed to 0.1%) and temperature-independent paramagnetism (TIP) were included according to $\chi_{calc} = (1 - PI)\chi + PI \times \chi_{mono} + TIP$. Before simulation, the experimental data were corrected for TIP. Full-matrix diagonalization of exchange coupling and Zeeman splitting was performed with the *julX* program.[14]

**Synthesis of the Ligand 2-(1-(2-Hydroxyethyl)-1*H*-pyrazol-3-yl)phenol ($H_2L$).** 1-(2-Aryl)-3-dimethylaminoprop-2-enone was synthesized by variation of the known literature procedure[28] at ambient pressure with elongated reaction times (45 min). One equivalent of the precursor was added to a solution of 2-hydroxyethylhydrazine (4 equiv) in methanol (100 mL), and the reaction mixture was heated to reflux for 3 h. The solvent was removed under reduced pressure, and the residue was transferred into ice water. HCl was added until a clear solution was obtained, and the solution was then extracted with dichloromethane. The combined extracts were dried over $MgSO_4$, and the solvent was removed under reduced pressure. After purification via column chromatography over silica gel with an ethyl acetate/pentane (1:1) mixture as eluent the product was obtained as a colorless solid. A batch of 39 mmol of 1-(2-aryl)-3-dimethylaminoprop-2-enone yielded 12.7 mmol, 33%. $^1$H NMR (300 MHz, $CDCl_3$, 300 K): $\delta$ = 4.04 (t, $^3J_{H,H}$ = 5.3 Hz, 2H, $CH_2$), 4.31 (t, $^3J_{H,H}$ = 5.3 Hz, 2H, $CH_2$), 6.63 (d, $^3J_{H,H}$ = 2.5 Hz, 1H, $CH^{Pz}$), 6.91 (dt, $^3J_{H,H}$ = 7.7, 1.2 Hz, 1H, CH), 7.02 (dd, $^3J_{H,H}$ = 8.3, 1.2 Hz, 1H, CH), 7.21 (dt, $^3J_{H,H}$ = 8.3, 1.2 Hz, 1H, CH), 7.52 (d, $^3J_{H,H}$ = 2.5 Hz, 1H, $CH^{Pz}$), 7.56 (dd, $^3J_{H,H}$ = 7.7, 1.2 Hz, 1H, CH). $^{13}$C NMR (75 MHz, $CDCl_3$, 300 K): $\delta$ = 54.4 ($CH_2$), 61.5 ($CH_2$), 102.4 (CH), 116.8 ($C_q$), 117.1 (CH), 119.5 (CH), 126.4 (CH), 129.3 (CH), 131.6 (CH), 152.0 ($C_q$), 156.7 ($C_q$). Mp: 91 °C. MS (EI+): $m/z$ (rel. intensity) = 204 (100) $[M]^+$, 173 (85) $[M - CH_2OH]^+$.

**Synthesis of $[Co_4(MeOH)_4(L)_4]$ (1).** Under inert conditions $Co(ClO_4)_2 \cdot 6H_2O$ (180 mg, 0.5 mmol) was added to a solution of the ligand $H_2L$ (100 mg, 0.5 mmol) in dry methanol (20 mL). Then $NEt_3$ (0.14 mL, 1 mmol) in dry methanol (5 mL) was added dropwise to the reaction mixture, affording a brown precipitate almost immediately. The precipitate was collected by filtration, washed with methanol, and dried in vacuum. The resulting powder was then dissolved in $CH_2Cl_2$ (20 mL) and layered with *n*-hexane. Brown crystals of the product $[Co_4(MeOH)_4(L)_4]$ (**1**) were separated after several days in the glovebox. MS (ESI+, MeCN): $m/z$ (rel. intensity) = 1045.2 (100) $[M - 4(MeOH) + H]^+$. IR (KBr): $\tilde{\nu}$ = 3107 (w), 3063 (w), 2914 (br), 2862 (m), 2790 (br), 2569 (w), 1597 (s), 1555 (m), 1516 (s), 1497 (s), 1466 (s), 1443 (s), 1412 (m), 1370 (w), 1351 (w), 1312 (vs), 1252 (m), 1227 (m), 1201 (m), 1156 (w), 1130 (s), 1086 (m), 1065 (s), 1032 (m), 959 (w), 929 (w), 883 (m), 847 (m), 746 (s), 688 (m), 645 (w), 614 (w), 570 (m), 546 (m), 446 (s) $cm^{-1}$. Anal. Calcd (%) for $C_{48}H_{56}Co_4N_8O_{12}$: C 49.16, H 4.81, N 9.55. Found: C 48.82, H, 4.67, N 9.62. After thermal treatment in the TGA apparatus a sample that was heated to 700 K showed the loss of all four MeOH ligands (mass loss: exp. 10.8%, calc. 10.9%). Anal. Calcd (%) for $C_{44}H_{40}Co_4N_8O_8$: C 50.59, H 3.86, N 10.73. Found: C 50.47, H, 3.91, N 10.65.

**X-ray Crystallography.** Crystal data and details of the data collections for **1** are given in Table 3 and in Supporting Information, Table S1. X-ray data were collected on a STOE IPDS II diffractometer (graphite monochromated Mo K$\alpha$ radiation, $\lambda$ = 0.71073 Å) by use of $\omega$ scans at −20 °C. Measurements at temperatures below −20 °C proved to be impossible due to disaggregation and loss of crystallinity of the single crystals. The structure was solved by direct methods and refined on $F^2$ using all reflections with SHELX-97.[29] The non-hydrogen atoms were refined anisotropically. Most hydrogen atoms were placed in calculated positions and assigned to an isotropic displacement parameter of 1.2/1.5 $U_{eq}$(C). The positional parameters of the oxygen-bound hydrogen atoms were refined by using DFIX restraints ($d_{O-H}$ = 0.82 Å). A fixed isotropic displacement parameter of 0.08 Å$^2$ was assigned to those hydrogen atoms. Face-indexed absorption corrections were performed numerically with the program X-RED.[30]

**Table 3. Crystal Data and Refinement Details for Complex 1**

| | 1 |
|---|---|
| empirical formula | $C_{48}H_{56}Co_4N_8O_{12}$ |
| formula weight | 1172.73 |
| crystal size [mm$^3$] | 0.27 × 0.23 × 0.10 |
| crystal system | monoclinic |
| space group | $P2_1/c$ |
| $a$ [Å] | 17.5372(7) |
| $b$ [Å] | 34.0208(10) |
| $c$ [Å] | 16.9603(7) |
| $\alpha$ [deg] | 90.00 |
| $\beta$ [deg] | 92.167(3) |
| $\gamma$ [deg] | 90.00 |
| $V$ [Å$^3$] | 10111.8(7) |
| $Z$ | 8 |
| $\rho$ [g/cm$^3$] | 1.541 |
| $F(000)$ | 4832 |
| $\mu$ [mm$^{-1}$] | 1.359 |
| $T_{min}/T_{max}$ | 0.6595/0.8188 |
| $\theta$ range [deg] | 1.31−25.74 |
| $hkl$ range | ±21, −41 to 37, ± 20 |
| measured refl | 116 377 |
| unique refl [$R_{int}$] | 19 035 [0.1003] |
| observed refl ($I > 2\sigma(I)$) | 11 871 |
| data/restraints/param | 19035/8/1328 |
| goodness−of−fit ($F^2$) | 1.026 |
| $R1$, $wR2$ ($I > 2\sigma(I)$) | 0.0604, 0.1016 |
| $R1$, $wR2$ (all data) | 0.1130, 0.1163 |
| resid el dens [e/Å$^3$] | −0.321/0.489 |

## ■ ASSOCIATED CONTENT

### Supporting Information

Experimental details; additional magnetic data for **1** and **1***; crystallographic data with bond lengths and angles. This material is available free of charge via the Internet at http://pubs.acs.org. CCDC-969653 contains the supplementary crystallographic data for this Paper. These data can be obtained free of charge from The Cambridge Crystallographic Data Centre via www.ccdc.cam.ac.uk/data_request/cif.

## ■ AUTHOR INFORMATION

### Corresponding Author

*E-mail: franc.meyer@chemie.uni-goettingen.de. Phone: +49 551 3933012. Fax: +49 551 3933063.

### Notes

The authors declare no competing financial interest.

## ■ ACKNOWLEDGMENTS

Financial support by the Deutsche Forschungsgemeinschaft (SFB 602, Project A16) is gratefully acknowledged.

## REFERENCES


(1) Jeon, I.-R.; Clerac, R. *Dalton Trans.* **2012**, *41*, 9565−9686.
(2) Sato, Y.; Ohkoshi, S.; Arai, K.; Tozawa, M.; Hashimoto, K. *J. Am. Chem. Soc.* **2003**, *125*, 14590−14595.
(3) Liu, C.-M.; Zhang, D.-Q.; Zhu, D.-B. *Chem. Commun.* **2008**, 368−370.
(4) Hao, Z.-M.; Zhang, X.-M. *Dalton Trans.* **2011**, 2092−2098 and references therein.
(5) Song, Y.-M.; Luo, F.; Luo, M.-B.; Liao, Z.-W.; Sun, G.-M.; Tian, X.-Z.; Zhu, Y.; Yuan, Z.-J.; Liu, S.-J.; Xu, W.-Y.; Feng, X.-F. *Chem. Commun.* **2012**, *48*, 1006−1008.
(6) (a) Motreff, A.; Correa da Costa, R.; Allouchi, H.; Duttine, M.; Mathonière, C.; Duboc, C.; Vincent, J.-M. *Inorg. Chem.* **2009**, *48*, 5623−5625. (b) Motreff, A.; Correa da Costa, R.; Allouchi, H.; Duttine, M.; Mathonière, C.; Duboc, C.; Vincent, J.-M. *J. Fluorine Chem.* **2012**, *134*, 49−55.
(7) Demeshko, S.; Leibeling, G.; Dechert, S.; Meyer, F. *Dalton Trans.* **2006**, 3458−3465.
(8) Das, A.; Klinke, F. J.; Demeshko, S.; Meyer, S.; Dechert, S.; Meyer, F. *Inorg. Chem.* **2012**, *51*, 8141−8149.
(9) Murrie, M.; Teat, S. J.; Stoeckli-Evans, H.; Güdel, H. U. *Angew. Chem., Int. Ed.* **2003**, *42*, 4653−4656.
(10) (a) Moubaraki, B.; Murray, K. S.; Hudson, T. A.; Robson, R. *Eur. J. Inorg. Chem.* **2008**, 5425−4529. (b) Galloway, K. W.; Whyte, A. M.; Wernsdorfer, W.; Sanchez-Benitez, J.; Kamenev, K. V.; Parkin, A.; Peacock, R. D.; Murrie, M. *Inorg. Chem.* **2008**, *47*, 7438−7442. (c) Guedes, G. P.; Soriano, S.; Comerlato, N. M.; Speziali, N. L.; Lahti, P. M.; Novak, M. A.; Vaz, M. G. F. *Eur. J. Inorg. Chem.* **2012**, 5642−5648.
(11) (a) Scheurer, A.; Ako, A. M.; Saalfrank, R. W.; Heinemann, F. W.; Hampel, F.; Petukov, K.; Gieb, K.; Stocker, M.; Müller, P. *Chem.—Eur. J.* **2010**, *16*, 4784−4792. (b) Zhang, S.-H.; Zhang, Y. D.; Zou, H. H.; Guo, J. J.; Li, H. P.; Song, Y.; Liang, H. *Inorg. Chim. Acta* **2013**, *396*, 119−125.
(12) Isele, K.; Gigon, F.; Williams, A. F.; Bernardinelli, G.; Franz, P.; Decurtins, S. *Dalton Trans.* **2007**, 332−341.
(13) Li, J.; Li, B.; Huang, P.; Shi, H.-Y.; Huang, R.-B.; Zheng, L.-S.; Tao, J. *Inorg. Chem.* **2013**, *52*, 11573−11579.
(14) Bill, E. *julX,* Magnetic Analysis Program; Max Planck Institute for Chemical Energy Conversion: Mülheim/Ruhr, Germany, **2008**.
(15) Aromí, G.; Batsanov, A. S.; Christian, P.; Helliwell, M.; Roubeau, O.; Timco, G. A.; Wimpenny, R. E. P. *Dalton Trans.* **2003**, 4466−4471.
(16) Zhang, K.; Dai, J.; Wang, Y.-H.; Zeng, M.-H.; Kurmoo, M. *Dalton Trans.* **2013**, *42*, 5439−5446.
(17) Volkmer, D.; Hommerich, B.; Griesar, K.; Haase, W.; Krebs, B. *Inorg. Chem.* **1996**, *35*, 3792−3803.
(18) Mydosh, J. A. *Spin Glasses: an Experimental Introduction;* Taylor & Francis: London, U.K., 1993.
(19) Kumar, A.; Tandon, R. P.; Awana, V. P. S. *J. Appl. Phys.* **2011**, *110*, 043926−43.
(20) Gatteschi, D.; Sessoli, R. *Angew. Chem., Int. Ed.* **2003**, *42*, 268−297.
(21) Van Vleck, J. H. *Phys. Rev.* **1941**, *59*, 724−729.
(22) Bindilatti, V.; Vu, T. Q.; Shapira, Y. *Solid State Commun.* **1991**, *77*, 423−426.
(23) Chiorescu, I.; Wernsdorfer, W.; Müller, A.; Bögge, H.; Barbara, B. *Phys. Rev. Lett.* **2000**, *84*, 3454−3457.
(24) Inagaki, Y.; Asano, T.; Ajiro, Y.; Narumi, Y.; Kindo, K.; Cornia, A.; Gatteschi, D. *J. Phys. Soc. Jpn.* **2003**, *72*, 1178−1183.
(25) Schenker, R.; Leuenberger, M. N.; Chaboussant, G.; Güdel, H. U.; Loss, D. *Chem. Phys. Lett.* **2002**, *358*, 413−418.
(26) Schenker, R.; Leuenberger, M. N.; Chaboussant, G.; Loss, D.; Güdel, H. U. *Phys. Rev. B: Condens. Matter Mater. Phys.* **2005**, *72*, 184403(10).
(27) Becker, H. G. O.; Berger, W.; Domschke, G.; Fanghänel, E.; Faust, J.; Fischer, M.; Gentz, F.; Gewald, K.; Gluch, R.; Mayer, R.; Müller, K.; Pavel, D.; Schmidt, H.; Schollberg, K.; Schwetlick, K.; Seiler, E.; Zeppenfeld, G. *Organikum,* 19th ed.; Johann Ambrosius Barth Verlag GmbH: Leipzig, Berlin, Heidelberg, 1993, p 668 ff.
(28) Plier, A.-K.; Glas, H.; Grosche, M.; Sirsch, P.; Thiel, W. R. *Synthesis* **2001**, 55−62.
(29) Sheldrick, G. M. *Acta Crystallogr.* **2008**, *A64*, 112−122.
(30) *X-RED;* STOE & CIE GmbH: Darmstadt, Germany, 2002.